Observations of Longitudinal Rolls in a Near Neutral Atmosphere[1]

BERNARD A. WALTER, JR. AND JAMES E. OVERLAND

Pacific Marine Environmental Laboratory/NOAA, Seattle, WA 98115

(Manuscript received 27 January 1983, in final form 25 August 1983)

ABSTRACT

Aircraft and satellite data are used to study the structure of longitudinal roll vortices in a nearly neutral ($z_i/L = -1.2$, where z_i is the inversion height and L is the Monin-Obukhov length) boundary layer over the ice-covered Bering Sea during February. Steam fog, formed over cracks and leads in the ice, was used as a tracer to delineate the various scales of roll motion seen in satellite images. The satellite information combined with aircraft data collected by the NOAA P-3 indicated the presence of a hierarchy of roll vortex motions. It is suggested that interactions of the various scales of motion resulted in certain scales dominating in one area and other scales dominating in another. Two-kilometer wavelength variations are attributed to the inflection point instability mechanism while 12–15 km variations seem to have been reinforced by the upstream topography on the Chukotka Peninsula. Organization of the fog banks on scales of 30 km was also present and may be attributable to resonant subharmonics of the basic boundary layer instability or to a mesoscale entrainment instability.

1. Introduction

This paper compares observations of longitudinal roll vortices from satellite imagery with nearly simultaneous observations from the NOAA P-3 research aircraft over the ice-covered northern Bering Sea in February, 1982 (Fig. 1). In the past, detection of secondary roll circulations in the atmospheric boundary layer from satellite imagery has usually depended on the presence of convective cumulus cloud streets situated above the areas of upward motion in the rolls during unstable conditions (Kuettner, 1959, 1971; Plank, 1966; Walter, 1980). In the present study the tracer used to delineate the rolls was "Arctic sea smoke" or steam fog which provided visual evidence of motions within the boundary layer. Conditions conducive to the formation of steam fog over the Bering Sea ice pack were caused by northerly winds advecting cold (approximately −20°C) Arctic air southward over the ice. Even though there was only a small percentage of open water (characterized by a sea surface temperature of −1.8°C) from cracks and leads in the ice, the very low saturation vapor pressure of the air due to its low temperature led to extensive fog formation. The planetary boundary layer was well-mixed up to 660 m and had near neutral stability. Using turbulent flux data from a gust probe system mounted on the aircraft, the Monin-Obukhov length L was calculated to be −551 m; thus, $-z_i/L = 1.2$, where z_i is the height of the inversion layer. The fluxes used to calculate L were means over the approximately 40 km legs and thus the effects of individual leads on heating the air are integrated over the whole leg. There was 10–12% of open water along each leg. This, combined with surface winds of 12.5 m s^{-1}, led to the formation of dynamically induced roll circulations in the boundary layer; these rolls swept the fog into linear features which marked convergent areas of the rolls and which were observed both in the satellite images (Fig. 2a, b) and by the P-3 aircraft.

Saunders (1964) determined the conditions necessary for the formation of steam fog and found that its characteristic form varied with the wind speed. His observations indicated that in moderate winds, steam fog commonly had a banded structure with the bands approximately aligned with the wind. Steam fog is usually regarded as a shallow phenomenon (~30–50 m deep), but Saunders states that in deep cold air the height of the fog can exceed 1500 m. In the present study the top of the fog bank was 700 m. Saunder's results applied to the conditions present here indicate that an air–sea temperature difference of at least −7°C was necessary for steaming to occur. Observed air–sea temperature differences were about −18.6°C; therefore, conditions were well within the regime required for steam fog formation.

The satellite imagery and aircraft data gave evidence for the coexistence of a number of scales of motion (Table 1), and the following sections will describe the sources of this evidence.

2. Experiment

The NOAA P-3 research aircraft flew crosswind and alongwind tracks during the period 2101 GMT 14

[1] Pacific Marine Environmental Laboratory Contribution No. 606.

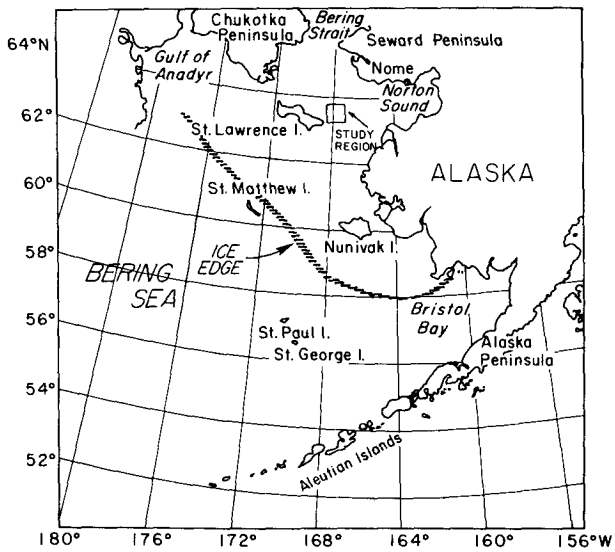

FIG. 1. Map of the Bering Sea showing the ice edge position and the study area.

February to 0020 GMT 15 February 1982 over the northern Bering Sea. The crosswind runs were approximately 48 km long. There were two positions for the crosswind tracks; the second was ~24 km south of the first. The first five crosswind tracks (2101 GMT–2150 GMT) are depicted as a solid track and the last ten (2215 GMT–0005 GMT) are shown as a dashed track in Figs. 2a and 2b. Runs were made at elevations of 42, 90, 195 and 340 m. The aircraft measurements began one hour and 42 minutes after the first satellite image (Fig. 2a) and continued until the time of the second satellite image (Fig. 2b).

Flight-level data from the P-3 included winds, temperature and dew-point temperature. Vertical profiles of these parameters were obtained by aircraft descent and ascent profiles. Measurements of heat, moisture and momentum flux were made by a gust probe system mounted on the P-3 (Bean *et al.*, 1975). Photos taken every five seconds by a 16 mm camera mounted in the nose of the aircraft provided important visual observations of the fog for comparison with the features seen in the satellite images.

For several days before 14 February, the Bering Sea was under the influence of a high-pressure system. Winds in the northern and central Bering were light and those in the southern Bering were from the NE at 10 m s^{-1}. The upper-level ridge began to shift westward toward Siberia near 1200 GMT 13 February and by 0000 GMT 14 February, northerly winds at ~10 m s^{-1} were present over most of the Bering Sea. By 0000 GMT 15 February (Fig. 3), the time of the aircraft flight, surface winds were N to NW at 12.5 m s^{-1} over the study area, and surface air temperatures had dropped 14°C in 18 hours to −20°C over the northern Bering Sea, which promoted ice production.

The evolution of the boundary layer structure was observed from the rawinsonde data at Nome. The 0000 GMT 14 February sounding showed that the atmosphere to 760 mb was saturated, and the lapse rate was moist adiabatic. The 1200 GMT 14 February sounding showed significant cooling (14°C at the surface and 8–10°C at 800 mb) from the previous sounding. The 0000 GMT 15 February sounding showed further cooling in the 980–750 mb layer and an inversion base at 920 mb.

Flight level data from the P-3 obtained during a descent profile before the low-level data collection runs and an ascent profile after the runs showed that the atmosphere was well-mixed up to the inversion where

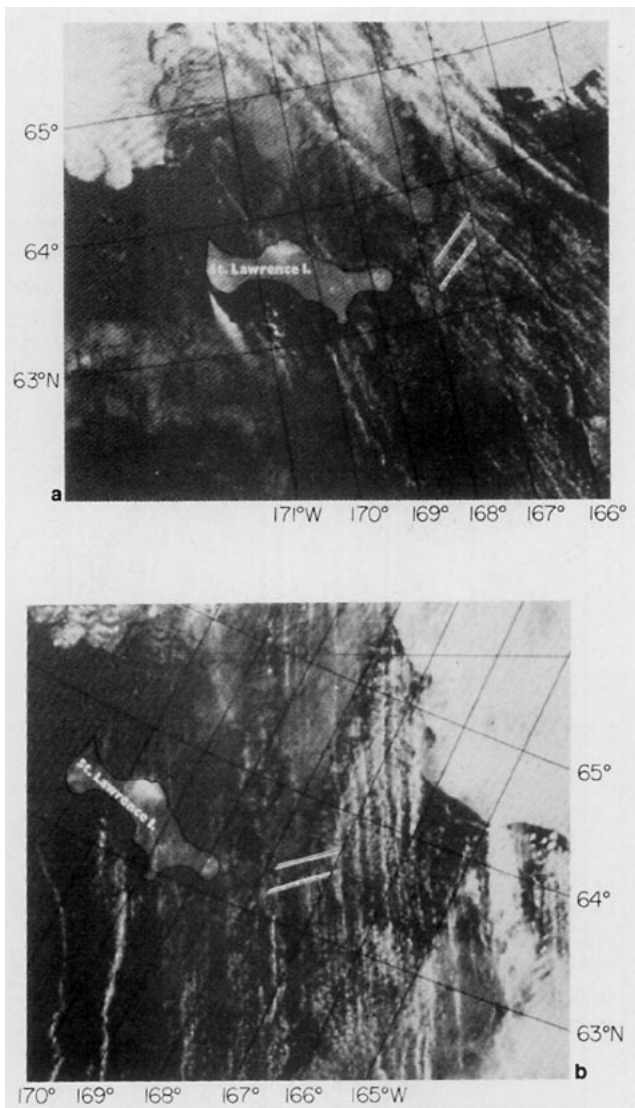

FIG. 2. (a) NOAA-6 AVHRR infrared image—1918 GMT 14 February 1982. (b) NOAA-7 AVHRR infrared image—0016 GMT 15 February 1982. The solid line shows the average flight track position for 2101–2150 GMT, the dashed line for 2215–0005 GMT.

TABLE 1. Summary of predominant scales seen in the aircraft time series data and satellite imagery.

Scale	Wavelength (km)	Evidence
α	30	Alternating patches of fog and clear areas each ~15 km wide in satellite images and aircraft film
β	12–15	Fog streets with origins near the Chukotka Peninsula in satellite photos and in filtered aircraft data
γ	5–6	Fog bands in satellite photos superimposed on α-scale and in filtered aircraft data
δ	1.3–1.7	In aircraft data time series and spectra
turbulence	0.35–0.75	In aircraft spectral data

the mean potential temperature in the mixed layer was 251.5K (Fig. 4a). The descent profile was done at a constant heading of 270° whereas the lower part of the ascent profile was done at a heading of 140° and the upper part at a heading of 75°. The potential temperature profile indicates that the inversion base height was at ~935 mb (660 m) which is in good agreement with the value of 920 mb obtained from the Nome sounding. The profiles of the u and v wind components (rotated into mean boundary layer wind coordinates) obtained during the descent and ascent profiles (Fig. 4b) showed that the wind speed was quite constant through the boundary layer. There was a counterclockwise rotation of ~18° in the wind direction as the aircraft descended through the inversion. Heading-dependent biases in the wind measurements have been removed.

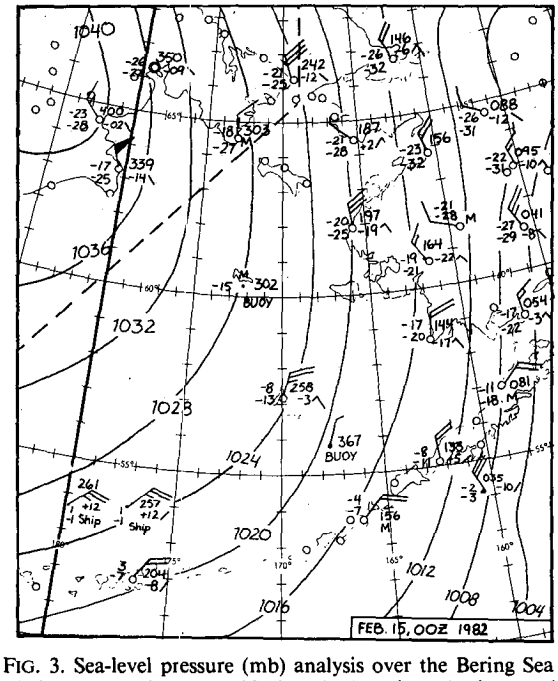

FIG. 3. Sea-level pressure (mb) analysis over the Bering Sea for 0000 GMT 15 February 1982. Standard station plotting symbols are used with each full tail barb equal to 10 kts and temperatures in °C.

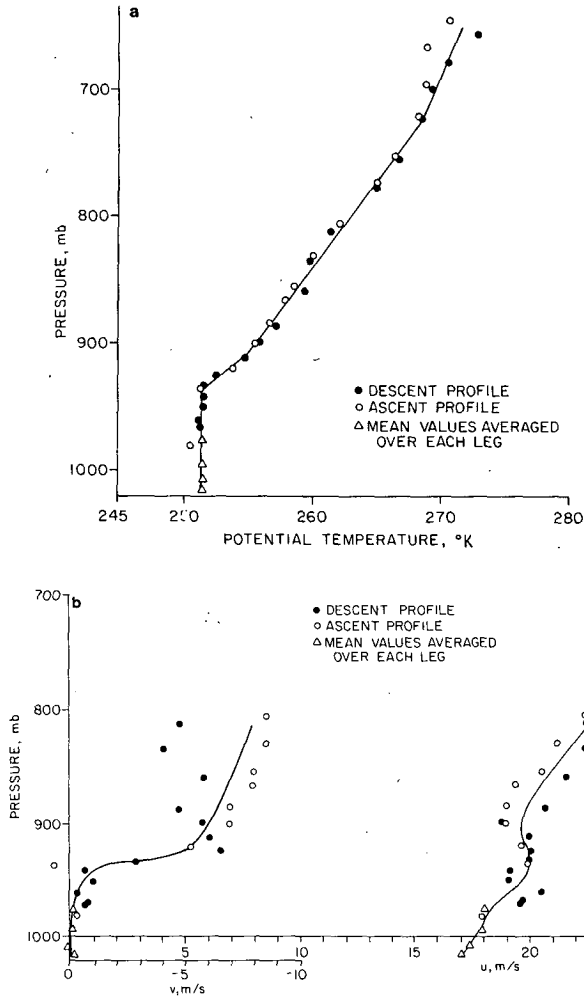

FIG. 4. (a) Vertical temperature structure of the boundary layer from P-3 profile data. (b) Vertical wind structure of the boundary layer from P-3 profile data; u and v velocity components are in a coordinate system where the x-axis is along the mean boundary layer wind direction (328°), the z-axis is vertical and the y-axis forms a right handed coordinate system.

3. Observations

a. Satellite measurements

The Advanced Very High Resolution Radiometer (AVHRR) sensors aboard the NOAA polar-orbiting satellites NOAA 6 and 7 were used to obtain information in the infrared on fog-band characteristics. The resolution of the AVHRR sensor is 1 km at nadir. Enlargements three times the original image were used

for making the measurements from images taken at 1918 GMT 14 February (Fig. 2a) and 0016 GMT 15 February (Fig. 2b). Special enhancements were used to resolve the fog with respect to the ice surface such that black indicated a temperature of −20°C and white indicated a temperature of −30°C.

The linear fog features seen in the satellite photos were organized on several scales with the angle of fog-band alignment, as measured from the images, at ~328–332°. This is very nearly parallel to the mean boundary layer wind direction. Figs. 5a and b are idealized sketches drawn from Figs. 2a and b, respectively, to point out some of the dominant scales seen in the satellite images. The broadscale features of the lower-level steam fog seemed organized into bands or patches of 15 to 20 km width with intervening clear areas of comparable width, thus giving a wavelength scale of 30–40 km (α-scale). Superimposed on the broader scale 30–40 km wavelength fog bands in Fig. 2a was a smaller scale band structure with a center-to-center separation of about 5 km (γ-scale). These bands can be seen as lighter gray (colder and higher) linear features on top of the darker gray (warmer and lower) wide fog bands.

Figure 2b has differences from the first image (Fig. 2a). There are two scales of well-defined linear features present (Fig. 5b). The smaller features are ~5.4 km apart which is similar to the scale in Figs. 2a and 5a. The wider features in the right half of Fig. 5b have a center-to-center spacing of 12 km (β-scale). There is a hint of this scale of organization in the area near 64.5°N, 167°W in Fig. 2a, but it is not until some time later (Fig. 2b) that it becomes well-defined.

Close inspection of the satellite images directly upstream from where the 12 km features were noted in Fig. 2b (off the top of the figure) revealed that these

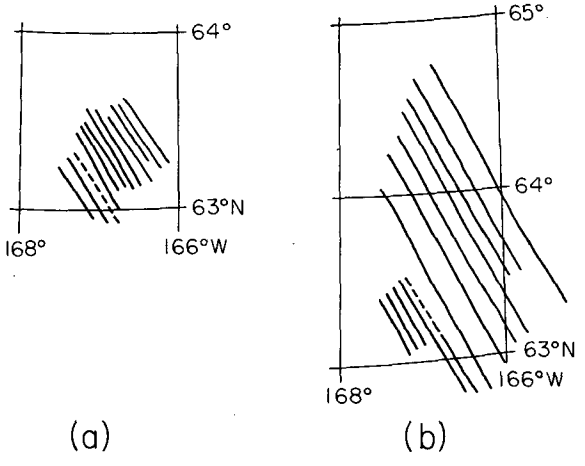

FIG. 5. (a) Scales of predominant linear features seen in 1918 GMT 14 February satellite image. Lines are approximately 4–5 km apart. (b) Scales of predominant linear features seen in 0016 GMT 15 February satellite image. Lines are approximately 5 km and 12–15 km apart.

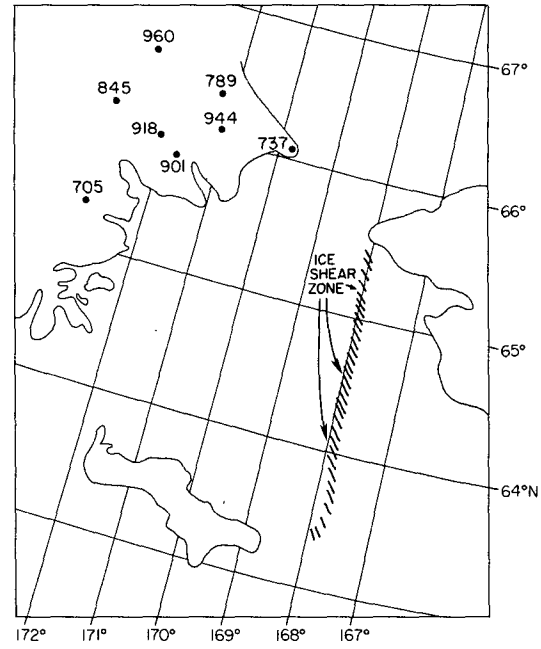

FIG. 6. Map showing mountain peaks (heights in meters) on Chukotka Peninsula and the location of the ice shear zone.

wavelengths were established far upstream along the coastline of the Chukotka Peninsula near 65.5–66.0°N, 170–171°W (Fig. 6). In this area, faint lines of fog delineate preexisting band structure with 12–15 km wavelength. These faint fog lines were evident near the coast as early as 1420 GMT 14 February as the cold air from Siberia began to flow southward over the ice pack. It was only when the air had passed over a shear zone in the ice pack (Fig. 6), where the ice was broken, that enough moisture was transferred to the boundary layer to form fog dense enough to more clearly define the rolls and the 12 km organization.

b. P-3 aircraft observations

Time series of wind direction at 42, 90 (Fig. 7a), 195 and 340 m also show the existence of different scales of motion. Examination of the spectra of the vertical velocity variations (w') measured by the gust probe system on the P-3 show an approximately linear increase with increasing height of the wavelength of the maximum energy eddies (Fig. 8). Results agree well with those of Nicholls and Readings (1981) and Nicholls and LeMone (1980). Dominant wavelengths at 340 m height are at λ = 1280 m or about twice the inversion height whereas at 90 m height they are at 300–500 m.

Composite spectra of the u' and v' variations (parallel and perpendicular, respectively, to the mean boundary layer wind direction) were formed by averaging spectra of individual legs at each height (three legs at 340 m and 195 m, eight legs at 90 m and two legs at 42 m).

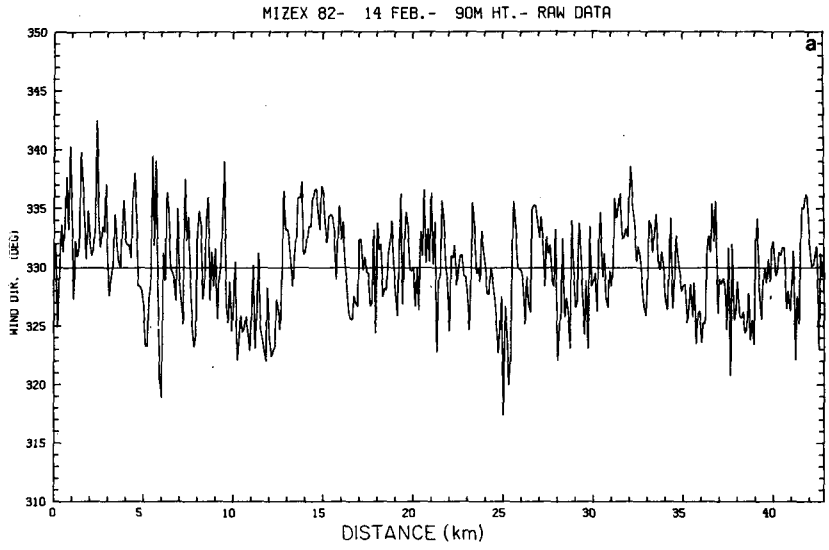

FIG. 7a. Example of time series of wind direction from P-3. Sample was from a height of 90 m and at 2122–2129 GMT 14 February. Mean direction for the sample was 330°. Scale at the bottom shows distance in km.

The u' spectra (Table 2) show a 1280 m peak at the top three levels, and the v' spectra show peaks in the range 1.0–1.7 km. This scale of variability in the data, near 1300–1700 m (δ-scale), is on the order of twice the boundary layer depth and is related to the existence of dynamically induced roll vortices in the boundary layer, as will be shown later.

The spectra tend to exhibit a bimodal nature in that along with this roll wavelength signature there is a smaller or "turbulent" scale peak. This is consistent with the results of LeMone (1976). The scales of motion on the order of several hundred meters at low levels are due to buoyant eddies produced as the air passes over open leads. As these buoyant plumes or bubbles rise, they grow in width which is reflected by the fact that the turbulent scale peak increases with height for the u' and v' spectra.

It is not possible to determine the 12 and 5–6 km contributions to the variability of different parameters because of the shortness of the legs and the fact that, due to smoothing, the longest wavelength contributed by the Fast Fourier Transform (FFT) to the spectrum is about 5.1 km. There does not appear to be any low-frequency contribution to the velocity spectra, but the spectra of the variations of both temperature and moisture at a height of 340 m do show a large amount

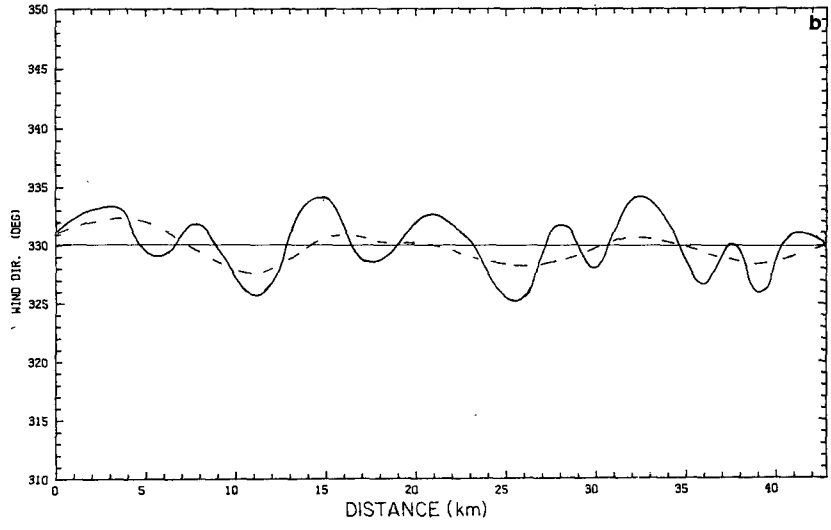

FIG. 7b. Filtered time series showing γ-scale variations (solid line) superimposed on β-scale variations (dashed line).

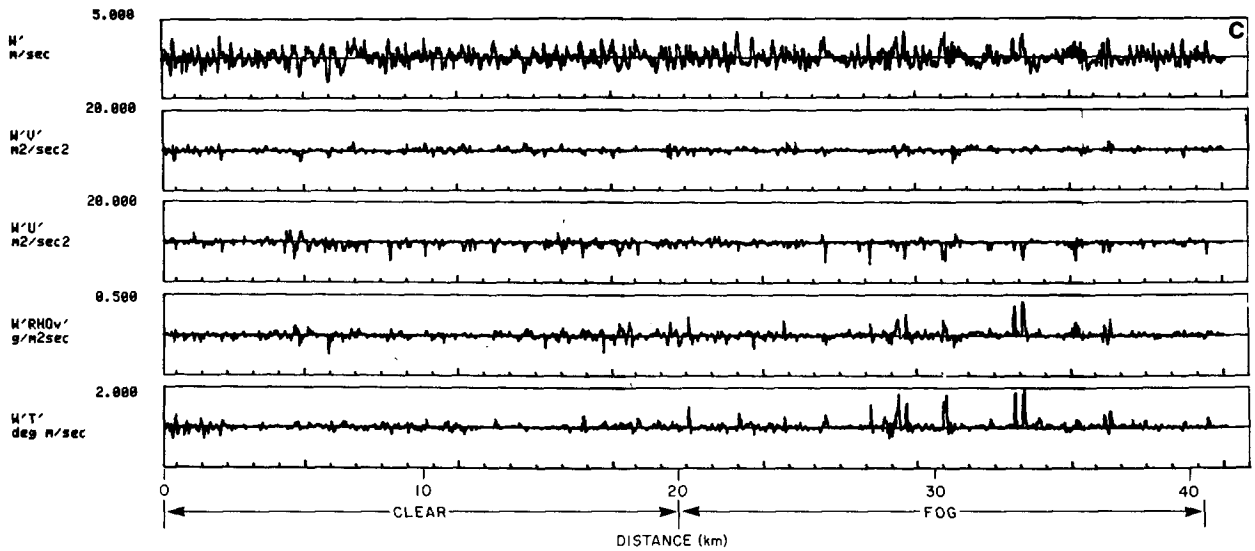

FIG. 7c. Time series of vertical velocity variations (w'), momentum flux ($\overline{u'w'}$ and $\overline{v'w'}$), moisture flux ($\overline{\rho_v' w'}$) and heat flux ($\overline{T'w'}$) for the period shown in (a).

of energy at the 5.1 km wavelength. Filtering the data brings out several predominant scales. Applying a low-pass filter with a 10 km cutoff to the time series in Fig. 7a shows the presence of the 12–15 km variations (dashed line in Fig. 7b) which were also noted in the satellite imagery. Superimposed on these are 5–6 km variations (solid line in Fig. 7b) which were also noted in the satellite imagery.

Photographs taken every five seconds by the nose camera on the aircraft showed good correlation with the broadscale location and width of the fog bands and clear areas seen in the satellite images. For example, by averaging over the crosswind legs, it was found that the broadscale fog band widths were about 13 km and the clear areas about 15 km (α-scale). For the particular run shown in Fig. 7a, the first 20 km was clear and the rest of the run was in fog. The difference in the temperature flux ($\overline{T'w'}$) and moisture flux ($\overline{\rho_v' w'}$) traces in the two regions (Fig. 7c) is characterized by a larger variability in the fog region.

Examination of the surface temperature time series obtained from a downward looking PRT-5 infrared radiometer shows that the total amount of open water along runs at 42 and 90 m in clear air was essentially the same as that along runs in fog. The steam fog was optically thin enough to enable the PRT-5 to detect differences in surface temperatures. This lends credence to the argument that the overall distribution of the fog banks was due to dynamics rather than the presence of fewer leads along the clear areas and more leads along the fog areas.

Careful observations of film taken at an altitude of 340 m, inside the fog, show modulations of light intensity (Fig. 9) on a scale of approximately every eight frames (40 sec) or 4 km. This may reflect the existence of γ-scale linear bands which were superimposed on the 30 km wavelength features. Observations from an aircraft vertical profile indicated that the 5–6 km features (as shown in Fig. 9) had tops near 1000 m, whereas the height of the fog in the valleys between these features was near 700 m or about the height of the inversion. It should be noted that the 5–6 km features were continuous with the lower level banks of ground fog and were not a separate cloud layer above the α-scale bands. The filtered time series in Fig. 7b show that the 5–6 km variations existed even at the 90 m level.

4. Discussion

There are several problems involved with attempting to correlate specific features seen in satellite images with those seen in aircraft measurements; these include nonstationarity of the features, resolution limitations of the satellite data and the shift in position of the aircraft track. However, we believe it is possible to make several general statements about the overall features of the flow field.

Comparison of the present study with previous observations and theoretical results for roll vortices in a neutral boundary layer shows some areas of agreement. The geostrophic wind (~800 m height) blew from 346° at about 21 m s^{-1}; thus the fog bands were at a 16–18° angle to the left of the geostrophic wind, as predicted by theory and observed in previous studies. Observations in the atmosphere by Plank (1966) and LeMone (1973) gave 15° for near-neutral conditions. Laboratory results by Faller (1963) showed orientation angles of 10–17° to the left of the gradient flow with an average of 14.5°. Theoretical studies by Stuart in

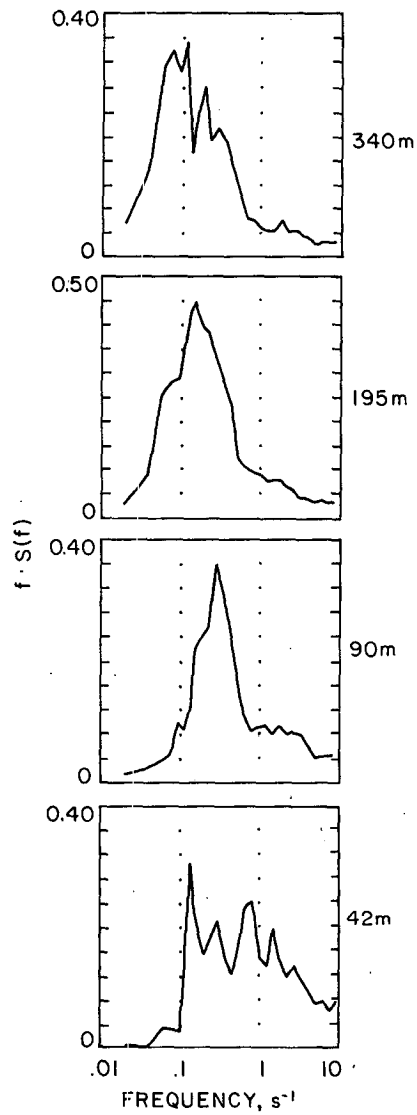

FIG. 8. Vertical velocity (w') spectra as a function of height.

Gregory *et al.* (1955) gave an orientation of 14°, while Brown's (1972) solutions for neutral conditions predicted 18°.

The 1300–1700 m wavelengths seen in the time series together with an inversion height of 660 m from the aircraft profiles give an aspect ratio of 2.0–2.6, which is an excellent agreement with previous atmospheric observations (Kuettner, 1971; LeMone, 1973) and theoretical results (Brown, 1970, 1972). Calculation of the Reynolds number, using the expression given by Brown (1970),

$$\mathrm{Re} = \frac{2V_g}{f\delta_i}$$

gives a value of Re = 2498, where V_g is geostrophic wind speed, f the Coriolis parameter, $\delta_i = 0.196z_i$ (LeMone, 1973) and $z_i = 660$ m. This value for Re is well in the supercritical range where the inflection point instability mechanism dominates. Even though the observed mean (i.e., in equilibrium with the rolls) velocity profile exhibited very little speed shear, there was a significant direction shear (~18°) at the inversion indicating the presence of an inflection point instability. The equilibrium mean velocity profile corresponds to those predicted by Brown (1972) for boundary layers containing rolls.

LeMone (1973) found that roll mean structure and amplitude were well described by the inflection point instability models, but that the magnitude of the observed roll circulation was up to 40% larger than the predicted value for rolls obtaining energy from wind shear alone. She concluded that this underestimate was most likely the result of the large contribution of buoyancy to the observed roll energy. Most of the cases studied by LeMone had values of $-z_i/L$ in the range of 7–10 and thus, buoyancy would play a much larger part in roll energetics than the present case where $-z_i/L = 1.2$ and mechanical mixing dominates.

The 12–15 km variations were seen in both satellite data (Fig. 5b) and aircraft time series (Fig. 7b). As mentioned earlier, in the region where the bands with 12–15 km spacing were seen in the satellite photos, it was possible to trace the genesis of individual fog bands to individual peaks upstream on the Chukotka Peninsula. The mountains on the Peninsula are separate peaks with heights on the order of 950 m. Thus, there may be an influence of this upstream topography in reinforcing these fog bands over the study area. Other instances of upstream topography possibly influencing cloud street spacing have been noted by Higuchi (1963), Asai (1966) and Tsuchiya and Fujita (1967) over the Sea of Japan during cold air outbreaks. Holroyd (1971) also observed large-scale cloud bands over the Great Lakes during what he called "enlarged lake storms" and attributed their existence to thermally induced convection from bays or frictional differences between land and water surfaces. Thus, both in the highly convective situations just noted and in the near neutral conditions present over the Bering Sea, the potential exists for strong upstream orographic dynamic or ther-

TABLE 2. Wavelengths of spectral peaks in the composite v' and u' spectra for each height, where u' variations are in the alongwind and v' in the crosswind direction.

Height	Spectral peaks (m) v'	Spectral peaks (m) u'
340	1710 and 732	1280 and 732
195	1280 and 732	1280 and 853
90	1020 and 512	1280, 853 and 512
42	853 and 333	1710 and 427

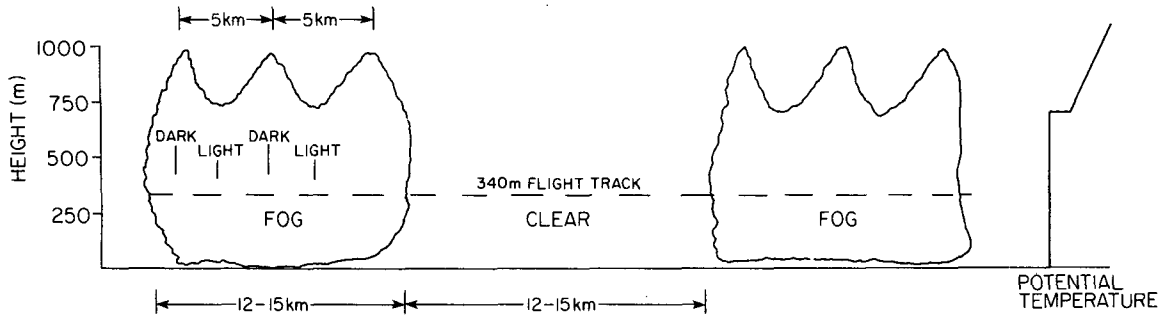

FIG. 9. Schematic diagram showing cross section of broad-scale fog banks with 5 km-scale features superimposed.

mal effects to either impose a particular scale of forcing on the flow, which would not otherwise be present, or to reinforce a particular instability mode.

Although it does not appear in the satellite imagery as a pronounced linear feature, there tends to be some organization of the fog and clear areas which exhibits a scale of variability on the order of 25–30 km (i.e., 12–15 km clear, 12–15 km fog). Variability on this scale is also present in the aircraft film observations. One hypothesis is that the scale of variability on the order of 25–30 km (and also 12–15 km) may be due to resonant subharmonics of the basic boundary layer instability.[2]

Another possible origin of the 30 km variations may be related to recent work by Fiedler (1982). He has shown that variations with a wavelength on the order of 30 km may be caused by a mesoscale entrainment instability (MEI) in which mesoscale fluctuations in the mixed layer are generated by the modulation of the entrainment of inversion air into the mixed layer. The criterion for the generation of unstable modes at these scales is that the potential temperature gradient in the inversion exceed approximately 10K km^{-1}. The gradient in the present case (Fig. 4a) was on this order and thus the α-scale variability noted here may be due to a MEI.

In addition to the 1.3–1.7 km, the 12–15 km and the 25–30 km scales of variability, there were 5–6 km-scale linear features superimposed on the broadscale fog banks observed in the satellite imagery (Fig. 2a, b). Modeling results of Mason and Sykes (1980), although applicable to strictly neutral conditions with no addition of heat, give insight into the roll structure present in the observations discussed above. They obtained large-scale rolls extending to heights of several kilometers, but indicated that interaction with smaller scale variations led to irregular flow patterns. Thus, the various scales observed may arise from the interaction of a hierarchy of scales of motion. The sketch in Fig. 10 shows the observed combined effect of the different scales of variability. The underlying 1.3–1.7 km wavelength rolls due to the inflection point instability are present in the well-mixed boundary layer in both fog and clear areas. Superimposed on this scale are variations with multiples of the 1.3–1.7 km variations. The presence of the 12 km wavelength structure in the right part of Fig. 5b was possibly initiated by the topography over the Chukotka Peninsula. This stronger circulation tended to dominate and suppress the effects of the 5–6 km and 30 km scale of variation (right side of Fig. 10) in the area downstream of the mountains. In the areas not influenced by the topography (left side of Figs. 5b and 10), the 5–6 km scale dominated and the result was seen as linear features of this scale superimposed on the 12–15 km wide low-level fog banks.

Using variational methods, Busse (1970) derived bounds on the turbulent transport of momentum in a boundary layer with shear flow. The resulting vector field which maximized the transport of momentum (Fig. 3 in Busse, 1970) is suggestive of the proposed atmospheric flow field shown in Fig. 10.

5. Summary

By using fog as tracer it has been possible to study the characteristics of dynamically induced horizontal roll vortices in a neutral planetary boundary layer showing close agreement of the present observations with theory and previous observations. A combination of nearly simultaneous satellite and P-3 aircraft data delineates a hierarchy of wavelength scales of organized circulations in the boundary layer:

1) 25–30 km scale is possibly due to resonant subharmonics of smaller scale instabilities or to a mesoscale entrainment instability,

2) 12–15 km scale may be related to the influence of upstream topography,

3) 5–6 km variation is an intermediate scale which may be due to the irregularity in the roll structure strength,

[2] Brown, R., personal communication, 1983, Polar Science Center, JC-10, University of Washington, Seattle, WA 98195.

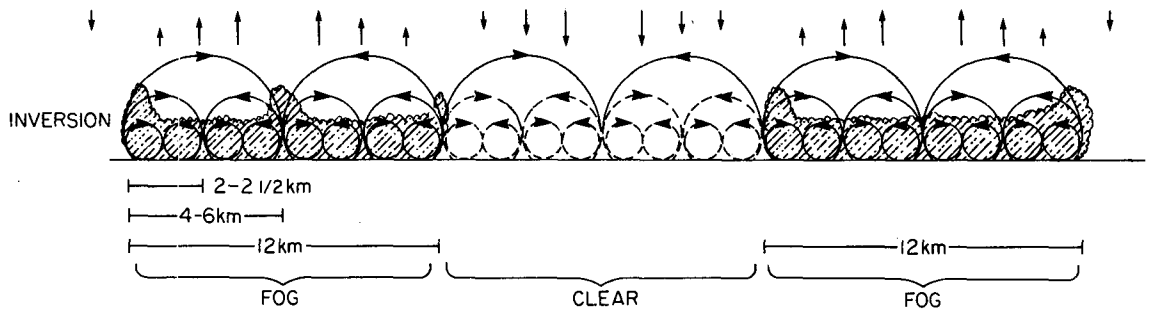

FIG. 10. Idealized cross section sketch showing a hierarchy of scales of motion acting to produce the observations from the satellite and P-3 data. The vertically pointing arrows located above the lower-level circulations are included to show the presence of the α-scale variations.

4) 1.3–1.7 km scale is that expected from the inflection point instability theory of the development of rolls in a neutral boundary layer.

5) 0.3–0.5 km scale is due to turbulent plumes.

Acknowledgments. This work is a contribution to the Marine Services Project at the Pacific Marine Environmental Laboratory. It was funded in part by Arctic Programs, Office of Naval Research. We thank the crew of the NOAA P-3 and personnel from the NOAA/ERL Gust Probe Group for collecting an excellent dataset and the Anchorage Ocean Services Unit of NWS for outstanding forecast support during the study. We also thank Bob Brown, Peggy LeMone and an anonymous reviewer for helpful comments and suggestions which have helped to strengthen the paper and acknowledge the assistance of Greg White at the NOAA Gilmore Creek, Alaska, satellite receiving station in processing the satellite images.

REFERENCES

Asai, T., 1966: Cloud bands over the Japan Sea off the Hokuriku district during a cold air outburst. *Pap. Meteor Geophys.*, **16,** 179–194.

Bean, B., C. Emmanuel, R. Gilmer and R. McGavin, 1975: The spatial and temporal variations of the turbulent fluxes of heat, momentum and water vapor over Lake Ontario. *J. Phys. Oceanogr.*, **5,** 523–531.

Brown, R., 1970: A secondary flow model for the planetary boundary layer. *J. Atmos. Sci.*, **27,** 742–757.

——, 1972: On the inflection point instability of a stratified Ekman boundary layer. *J. Atmos. Sci.*, **29,** 850–859.

Busse, F. H., 1970: Bounds for turbulent shear flow. *J. Fluid Mech.*, **41,** 219–240.

Faller, A., 1963: An experimental study of the instability of the laminar Ekman boundary layer. *J. Fluid Mech.*, **15,** 560–576.

Fiedler, B. H., 1982: Mesoscale entrainment instability as the cause of mesoscale cellular convection. Ph.D dissertation, Dept. of Astro-Geophysics, University of Colorado, 151 pp.

Gregory, N., J. Stuart and W. Walker, 1955: On the stability of three-dimensional boundary layers with application to the flow due to a rotating disk. *Phil. Trans. Roy. Soc., London* **A248,** 155–199.

Higuchi, K., 1963: The band structure of snowfalls. *J. Meteor. Soc. Japan,* **41,** 53–70.

Holroyd, E., 1971: Lake-effect cloud bands as seen from weather satellites. *J. Atmos. Sci.*, **28,** 1165–1170.

Kuettner, J., 1959: The band structure of the atmosphere. *Tellus,* **11,** 267–294.

——, 1971: Cloud bands in the earth's atmosphere: Observations and theory. *Tellus,* **23,** 404–425.

LeMone, M., 1973: The structure and dynamics of horizontal roll vortices in the planetary boundary layer. *J. Atmos. Sci.*, **30,** 1077–1091.

——, 1976: Modulation of turbulence energy by longitudinal rolls in an unstable planetary boundary layer, *J. Atmos. Sci.*, **33,** 1308–1320.

Mason, P., and R. Sykes, 1980: A two-dimensional numerical study of longitudinal roll vortices in the neutral atmospheric boundary layer. *Quart. J. Roy. Meteor. Soc.*, **106,** 351–366.

Nicholls, S., and M. A. LeMone, 1980: The fair weather boundary layer in GATE. II: The relationship of subcloud fluxes and structure to the distribution and enhancement of cumulus clouds. *J. Atmos. Sci.*, **37,** 2051–2067.

——, and C. J. Readings, 1981: Spectral characteristics of surface layer turbulence over the sea. *Quart. J. Roy. Meteor. Soc.*, **107,** 591–614.

Plank, V., 1966: Wind conditions in situations of patternform and non-patternform cumulus convection. *Tellus,* **18,** 1–12.

Saunders, P. M., 1964: Sea smoke and steam fog. *Quart. J. Roy. Meteor. Soc.*, **90,** 150–165.

Tsuchiya, K., and T. Fujita, 1967: A satellite meteorological study of evaporation and cloud formation over the western Pacific under the influence of the winter monsoon. *J. Meteor. Soc. Japan,* **45,** 232–250.

Walter, B., 1980: Wintertime observations of roll clouds over the Bering Sea. *Mon. Wea. Rev.*, **108,** 2025–2031.